International Journal of Civil Engineering (2019) 17:323–332
https://doi.org/10.1007/s40999-017-0278-4

RESEARCH PAPER

Seismic hazard assessment of arch dams via dynamic modelling: an application to the Rules Dam in Granada, SE Spain

Enrico Zacchei[1] · José Luis Molina[1] · Reyolando Manoel Lopes Rebello da Fonseca Brasil[2]

Received: 25 May 2017 / Revised: 8 November 2017 / Accepted: 9 December 2017 / Published online: 13 December 2017

Abstract
Dams are extremely strategic structures that must be carefully designed for human and environmental safety. This paper aims to analyse the influence of probabilistic and deterministic seismic hazards, defined for the site, on the singular points of the Rules dam in southern Spain. A comparison with the data from a recent seismogenic zone (2015) has been made; the adopted criteria for the comparison have been carefully explained. Seismic input from the Safety Evaluation Earthquake has shown that maximum accelerations are three times higher than the Spanish code value. Consequently, the stress has exceeded the maximum allowed tension, creating a number of plastic hinges. To consider the fluid–structure–foundation interaction, 2D and 3D mathematical models have been developed via finite element and gravity methods. A good calibration between the observations and modelling output has been obtained.

Keywords Dynamic analysis · Hydraulic structure · Rules arch-dam · Seismic hazard · Two- and three-dimensional models

Abbreviations

THA	Time-history analysis
PSHA	Probabilistic Seismic Hazard Assessment
DSHA	Deterministic Seismic Hazard Assessment
OBE	Operating basis earthquake
SEE	Safety evaluation earthquake
PSA	Pseudo-spectra acceleration
ZS	Seismogenic zones
IGN	National Geographic Institute
IAG	Andalusian Institute of Geophysics
PDF	Probability density function
PGA	Peak ground acceleration
ESM	Engineering strong-motion
UHS	Uniform hazard spectra
FEA	Finite element analysis

✉ José Luis Molina
jlmolina@usal.es

Enrico Zacchei
enricozacchei@gmail.com

Reyolando Manoel Lopes Rebello da Fonseca Brasil
reyolando.brasil@gmail.com

[1] Higher Polytechnic School of Ávila, University of Salamanca (USAL), 50 Hornos Caleros Avenue, 05003 Ávila, Spain

[2] Polytechnic School of São Paulo, University of São Paulo (USP), 380 Prof. Luciano Gualberto Avenue, 05508-010 São Paulo, Brazil

1 Introduction

This paper describes the seismic evaluation of the Rules dam (located in Granada, Spain), a concrete arch-gravity dam, via time-history analysis (THA). Probabilistic Seismic Hazard Assessment (PSHA) and Deterministic Seismic Hazard Assessment (DSHA) have been used to define the seismic data input. The former is necessary to calculate the Operating Basis Earthquake (OBE), which defines any low-level damage to the dam, whether insignificant or absent. The latter is used to calculate the Safety Evaluation Earthquake (SEE), which defines significant levels of damage, such as events resulting from uncontrolled water flow that has not been released, which could lead to catastrophic consequences. The main difference between the probabilistic and deterministic analyses is that the former considers the earthquake frequency, whereas the latter provides a straightforward framework for evaluating the worst possible case of ground motion. The Cornell Method [1] is the procedure that defines the PSHA; it is based on three assumptions: the events are independent and stationary in time; the probability distribution of the magnitude is defined by an exponential distribution, and the seismicity is uniformly

distributed in each seismogenic zone (in contrast to Kernel Method [2], which disregards the seismogenic zones). A DSHA considers the seismic-geological context and the historical earthquake data, which represent different ground motion accelerations. The current data analysis considers the dam location and any uncertainties of the procedure [3]. The probability density function (PDF) and the pseudo-spectra acceleration (PSA) for different return periods have been calculated; the results have been compared to similar results from a previous analysis. Some uncertainties of the PSHA are due to incorrect values from the catalogue. For example, different magnitudes are due to the existence of different types of seismic waves, equations and records. To perform an accurate analysis, the data must be corrected via homogenization, declustering and completeness [4]. These corrections have been explained below.

To evaluate the seismic response of dams, a mathematical model in two and three dimensions has been developed. This model consists of a 3D analysis that considers the block interactions and a 2D analysis that considers vertical and horizontal stresses. The vertical stresses have been calculated using the upstream and downstream faces of the dam wall. To account for the interaction between fluid–structure–foundation observed by the system, geometrical and material parameters have been considered.

The Rules dam was built in 2003, and the new seismogenic zones were created in 2015; as a result, the considerations exposed here may not have been considered in the original project. Many arch dams in the world may face similar problems. Therefore, seismic hazard reassessment is advisable, particularly for existing category A dams [5] in areas of high seismicity. Many important regions of the world are vulnerable to seismic activity; consequently, risk assessments must be made to ensure that vulnerable areas are protected.

2 Seismic risk analysis: explanation of criteria

2.1 Probabilistic seismic hazard analysis

The main characteristic of probabilistic seismic hazard analysis is that it considers earthquake frequency. The basic Cornell method is used in this study; it is based on the Poisson process and Gutenberg–Richter law [6, 7]. In this section, the probabilistic seismic hazard analysis and its chosen criteria will be explained. The new Seismogenic Zones (ZS) of the Iberian Peninsula, established in 2015, are also considered [8]; this map is formed by 55 superficial zones and four deep zones. Earthquakes have the same probability of occurrence at any point inside the zone regardless of its size. This is an important condition when applying the Cornell method, particularly since additional seismogenic zones exist in previous literature [9]. To start, hazard analysis from the historic catalogue must be examined. In this study, the Instituto Geográfico Nacional (IGN) catalogue has been used [10]. This catalogue contains information about the intensity, magnitude and depth of earthquakes in the Andalusia area. The relative range of the coordinates is − 8° to 0° (longitude) and 35° to 39° (latitude). There are other catalogues, e.g., Andalusian Institute of Geophysics (IAG) [11], that can be integrated if the data are incomplete. However, the authors determined that the IGN catalogue data and the number of the used zones are sufficient to carry out this analysis. To perform the probabilistic analysis, four attenuation relations (SP96, Am96, Am05, BT03) [12–15] have been used (see Table 1). The use of these attenuation equations is justified by the fact that they were calibrated using data from Italian records. Note that the Italian tectonic activity is the result of a somewhat similar geological context to that in our area of study [16]. In general, these equations have been largely used in the South-European context.

The homogenization of the magnitude was made to provide the unique moment magnitude (M_w); this is necessary because the data from the IGN catalogue contain five different magnitudes and macro-seismic intensity values. To perform this operation, updated equations and methods from recent literature have been used [17–19]. To use the Poisson process (independence between events), fore-shocks, after-shocks and swarms (in time and space) must be eliminated. The analysis of completeness must be made to correctly estimate the mean annual rate of exceedance (λ_c). This analysis considers the periods that contain an adequate number of seismic events. For example, in the uncorrected catalogue of this analysis, there are only 96 seismic events between 1406 and 1795, whereas in the period between 1796 and 2013, there are more than 16,795 events. If only 96 events were considered in a large period, λ_c would be underestimated. In Fig. 1a, 12,058 uncorrected events within a radius of 150 km from the case study (black point) are shown. To

Table 1 Attenuation equations applied to define the PSA (g)

Abbreviation	Complete definition of attenuation relationships[a]
Am05	$\mathrm{PSA} = 10^{\{a_1+a_2M_w+(a_3+a_4M_w)\log\sqrt{R_{jb}{}^2+a_5^2}\pm\sigma\}}$
Am96	$\mathrm{PSA} = 10^{\{C'_1+C_2M_s+C_4\log(R_{jb})\pm\sigma\}}$
SP96	$100\times\mathrm{PSA} = \omega 10^{\{a+b'M_s+c\log_{10}(R_{epi.}{}^2+h^2)^{1/2}\pm\sigma\}}$
BT03	$100\times\mathrm{PSA} = 10^{\{a(f)M_s+b(f)R_{hyp.}-\log_{10}R_{hyp.}+c_1(f)\pm\sigma\}}$

[a]The equations are for the rock sites. The coefficients $\{a_1, a_2, a_3, a_4, a_5, C'_1, C_2, C_4, \omega, a, b', c, h, a(f), b(f), c_1(f)\}$ of the attenuation relationships can be found in the literature [12–15]. In Am05, the faulting mechanism is not considered. In BT03, $R_{hyp.}$ (km) corresponds to the hypocentral-Rules dam distance. σ is the standard deviation defined in the text

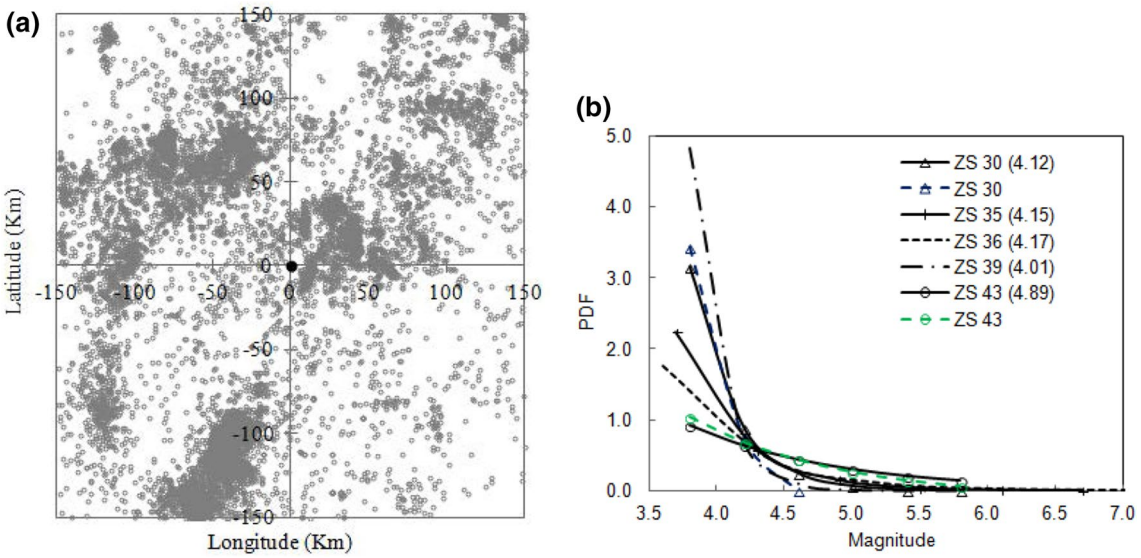

Fig. 1 Earthquakes within a radius of 150 km from the Rules dam (**a**) and probability density function for five seismogenic zones—its mean value is shown in brackets (**b**)

make these operations (catalogue declustering, homogenization and completeness) practical, only the events in the 11 seismogenic zones (Zesis) have been considered. These 11 zones are within a radius of 150 km, which is the recommended distance to adopt the attenuation equations. To eliminate the duplicates, there are some approaches suggested in the literature [20]. Blocks of events with the same latitude and longitude (or with an allowable displacement difference of 0.5 decimal degrees) were considered; later, the largest magnitude events were identified, and any events below this threshold magnitude were eliminated. The maximum reasonable time interval was 90 days. To perform the completeness analysis, the cumulative earthquakes-per-year method has been used. The method uses linear regressions by dividing the magnitude into variance groups, ΔM_w. For both cases (declustering and completeness), a visual method has been utilized. The Gutenberg and Richter exponential distribution was applied to define a (vertical intercept) and b (slope) parameters (see Table 2). The a-parameter represents the seismic activity; the greater the a-value is (in this analysis the range is 1.36–7.52), the higher the seismicity of the zone. In Table 2, the mean annual rate of exceedance, b-value, β-value, $m_{,\max}$ and $m_{,\min}$ are shown; λ_c depends on the earthquake's time distribution, completeness time interval and number of reported events. Thus, if λ_c increases, then the number of events increases, or the time interval decreases. The b value describes the relative likelihood of small and large earthquakes. In this analysis, this value ranges between 0.40 and 2.09. When the values have a shallow slope (approximately 0.40–0.97), the small earthquakes have a lower frequency compared to the strong earthquakes in the zone; thus, the seismic hazard is high in this case.

Table 2 Data of the probabilistic analysis

ZS	λ_c	b	β^a	$m_{,\max}$	ΔM_w	$m_{,\min}$	$\Delta\lambda_c$	Δb	$\Delta m_{,\max}$	$\Delta(\Delta M_w)$
29	0.241	0.91	2.08	6.8	0.40	3.6	− 0.05	0.11	− 0.2	0.00
30	0.086	1.37	3.16	4.6	0.20	3.8	− 0.03	− 0.11	0.4	0.20
34	0.296	0.83	1.92	6.7	0.30	3.7	− 0.10	0.17	− 0.1	0.00
35	0.556	0.97	2.24	6.7	0.30	3.7	0.02	0.15	0.1	0.00
36	0.159	0.76	1.75	6.8	0.40	3.6	− 0.02	0.22	− 0.2	0.00
37	0.546	1.10	2.54	5.4	0.20	3.8	− 0.16	0.06	1.4	0.00
38	0.453	0.82	1.88	6.6	0.20	3.8	− 0.14	0.14	0.1	0.00
39	0.113	2.09	4.82	5.0	0.20	3.8	− 0.03	− 0.75	1.7	− 0.10
40	0.441	0.93	2.14	6.1	0.30	3.7	− 0.31	0.01	0.4	0.00
43	0.659	0.40	0.92	6.2	0.20	3.8	0.23	0.67	0.8	0.00
55	0.667	0.94	2.17	6.8	0.40	3.6	− 0.04	0.09	− 0.1	− 0.10

[a] This value is defined by: $\beta = b\ln 10$

When b is approximately more than 1.00, the seismic hazard is low. The $m_{,max}$ and $m_{,min}$ values are needed to define the PDF and represent its upper and lower limits (see Fig. 1b). The PDF indicates the likelihood that a particular magnitude exceeds a certain $m_{,min}$. For ZS 30 and ZS 43 (dashed line), the PDF also has an upper limit $m_{,max}$. The upper and lower truncated curves likely have small magnitudes, and therefore, the curves are slightly higher. The PDF of ZS 39 is high; it is characterized by events that release energy from small earthquakes. Table 2 shows the values of this study; in the last four columns, the difference (Δ) between the data from this study and the Zesis study (the negative values indicate that the Zesis data are lower than our data) is provided, and some differences can be seen (values are underlined). When considering $\Delta m_{,max}$, the macroseismic intensity changes for a magnitude range of ±0.5, while the physical significance of $\Delta\lambda_c$ and Δb changes to ±0.15 and ±0.35, respectively.

The disaggregation analysis has been performed to separate the magnitude and distance contributions that generated acceleration. The values of the analysis are chosen according to the dam's fundamental period (T_d), return period (T_r) and Peak Ground Acceleration (PGA). The last parameter, obtained by software (Crisis) [21], differs greatly from the design values obtained by PSHA due to wide intervals of T_r. Therefore, the results depend on the first two periods. Three different return periods have been considered: 475-, 1000- and 5000-years; the following values are obtained as a result: $M_w = 4.7$ and $R_{epi.} = 7.5$ km (epicentral-site distance); $M_w = 5.9$ and $R_{epi.} = 7.5$ km; $M_w = 6.1$ and $R_{epi.} = 7.5$ km, respectively. The 1950-year period is a fourth return period that has been considered; it will not be shown in the PSHA since the PSA values are approximately 1.65 more than the values of the 475-year period.

2.2 Deterministic seismic hazard analysis

The deterministic seismic hazard analysis is needed to define the worst earthquake. Since the analysis does not consider the probability of occurrence (return period), it is convenient to consider the standard deviations (σ) of the attenuation equations. The standard deviation values used range from ±0.19 to ±0.26. For a strategic structure, such as a dam, the return period is generally very large. For this reason, the probabilistic analysis alone can be unreliable. A deterministic analysis should be carried out using the seismic-geological context [22] and the historical earthquake data. In Table 3, five controlling earthquakes were chosen according to the disaggregation analysis and the PGA obtained from the PSHA. The earthquake details have been taken from the Engineering Strong-Motion (ESM) database [23], and their analyses have been performed by software (Seismosignal) [24]. The recorded data have considered the three orientations (east–west, north–south and up–down), but only the heaviest results are shown (Table 3). The seismic events are superficial, e.g., the hypo-central distance (depth) is up to 30 km. The other four events are historical earthquakes in Spain.

3 Materials and methods

The mathematical model must be made in two and three dimensions because there is an interaction between arch and cantilever units. The actions create six components—three translational and three rotational (vertical movements and rotations in vertical tangential planes are neglected). The modelling is divided into three parts: 3D analysis considers the arch effects, 2D analysis studies the vertical and

Table 3 Series of records used in the analysis

Location	Date, time	M_w	M_s	Depth (km)	PGA (cm/s^2)	$R_{epi.}$ (km)
Messinia, Greece	13/09/1986, 17:24:34	5.9	5.8	27.6	234.04	6.625
Foligno, Italy	26/09/1997, 09:40:24	6.0	6.1	5.7	201.39	4.804
Medolla, Italy	29/05/2012, 07:00:02	6.0	5.9[a]	8.07	232.12	14.249
Adra, Spain	16/06/1910, 04:16:41	6.1	6.0[a]	–	–	6.82[a]
Alhama de Almería, Spain	22/09/1522, 10:00:00	6.5	6.5[a]	–	–	50.69[a]
Torrevieja, Spain	21/03/1829, 18:39:00	6.6	6.6[a]	–	–	174.63[a]
Málaga, Spain	09/10/1680, 07:00:00	6.8	6.8[a]	–	–	32.19[a]
Bjeliši, Montenegro	15/04/1979, 06:19:41	6.9	6.9	3.79	356.23	6.841
Pınarlar Köyü, Turkey	12/11/1999, 16:57:19	7.3	7.4	10.4	343.79	5.274

[a] Estimated values (representing an epicentral distance to the Rules dam and the surface-wave magnitude, M_s)

Additional important data are indicated as follows. Significant duration, D_{Ia} (sec): Greece = 5.13; Italy (1997) = 11.77; Italy (2012) = 11.96; Turkey = 10.98; Montenegro = 21.27. Distance between site and the surface projection of the fault, R_{jb} (km): Italy (1997) = 1.63; Italy (2012) = 9.4; Turkey = 8.64; Montenegro = 2.97. Style of fault ruptures that generate the seism: normal faulting in Greece and Italy (1997); thrust faulting in Italy (2012) and Montenegro; strike-slip faulting in Turkey

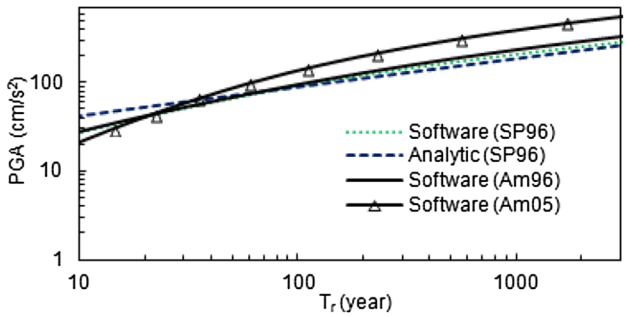

Fig. 2 PGA in function of the return period for the ZS 35 (site of the dam)

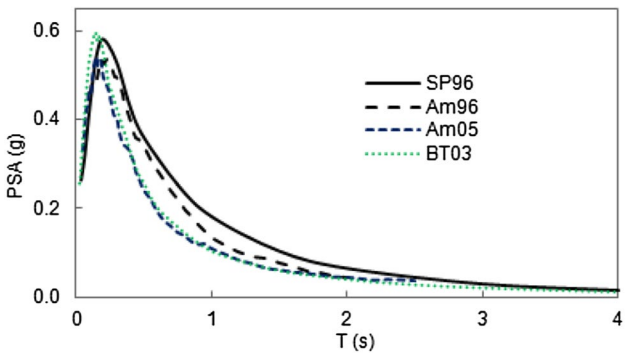

Fig. 3 Four synthetic spectra for 1950 years

horizontal stresses, and 2D analysis via the gravity method studies the stability (only some results will be shown). To consider the interactions among liquid, structure and rock observed by the system, geometry and material parameters have been specified. Certain earthquakes have been chosen to perform the THA. The vertical stresses (normal and principal) have been calculated in the upstream and downstream faces of the dam wall; therefore, the exceedance that produced the plastic hinges was estimated.

To design the structure, the SEE and OBE levels were defined and calculated via deterministic and probabilistic approaches, respectively [25]. In Fig. 2, the annual probability of exceedance from Crisis is shown for ZS 35. The differences between the curves mainly depend on the attenuation equations used and on their standard deviations, e.g., if the standard deviation decreases, then the return period increases. The standard deviation values used a range from ± 0.19 to ± 0.29. For the analysis, zero has been used, and the source has been approximated via a circular region with a 47-km radius. The solid-triangle curve points, shown in Fig. 2, are higher because the equation was not well-constrained for low magnitudes; therefore, the curve overestimates the acceleration with a higher T_r. In Fig. 3, the PSAs calculated using values obtained by disaggregation analysis are shown (the pair values, M_w and

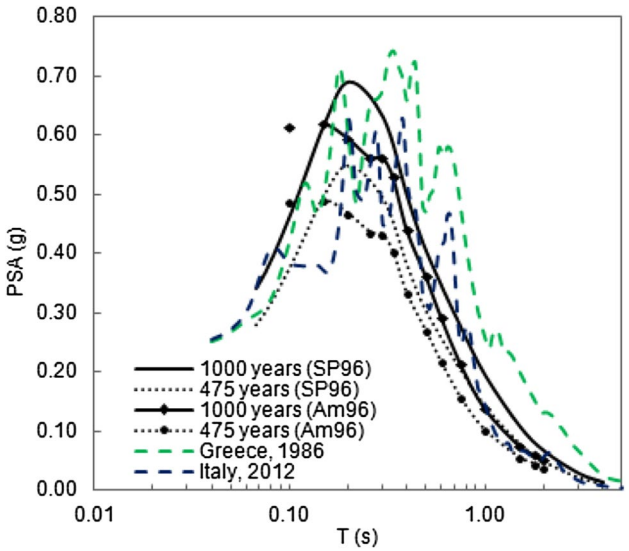

Fig. 4 Probabilistic spectra using T_r for 475 years and 1000 years, and two controlling earthquakes

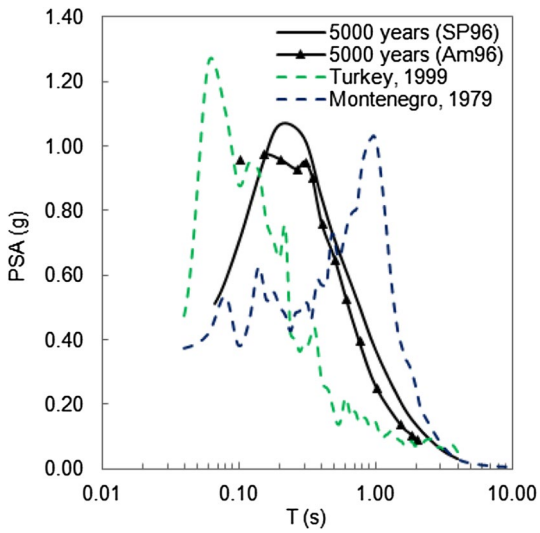

Fig. 5 Probabilistic spectra using T_r for 5000 years and two controlling earthquakes

R_{epi}., used are the same for the 5000-year period). Because of the limited interaction of the software, the curves refer exactly to the following return periods: 455-, 1023-, 1949- and 4835-years. This difference is irrelevant for the analysis of the output data. The attenuation equations do not use the same magnitude and distances; therefore, the values are estimated. The distances, shown in Fig. 3, are as follows: 5.5 km for Am96 and 10 km for BT03. The Uniform Hazard Spectra (UHS), which considered all the zones and four controlling earthquakes, are shown in Figs. 4 and 5. The UHS provides the accelerations, which depend on the structure periods (T) for a fixed return period. The PGA

for the 475-year return period in the analysis is 0.198 g (19.8% of gravity acceleration). This value concurs with literature [26]. The PGA for the 1000-year return period in the analysis is 0.252 g, which is the value used for the dam analysis. For the 5000-years return period, the PSA for $T = 0.25$ s is 0.928 g, which is similar to the deterministic PSA (1.00 g); this is because a probabilistic analysis for a large return period is unrealistic and often overestimated. In Fig. 6, the deterministic spectra obtained for four historical earthquakes, via two different attenuation relations, are shown. In the Spanish code, the PGA for this area is 0.17 g; however, in the full analysis, the soil with the greatest registered acceleration is 0.511 g, which is three times higher than the Spanish code.

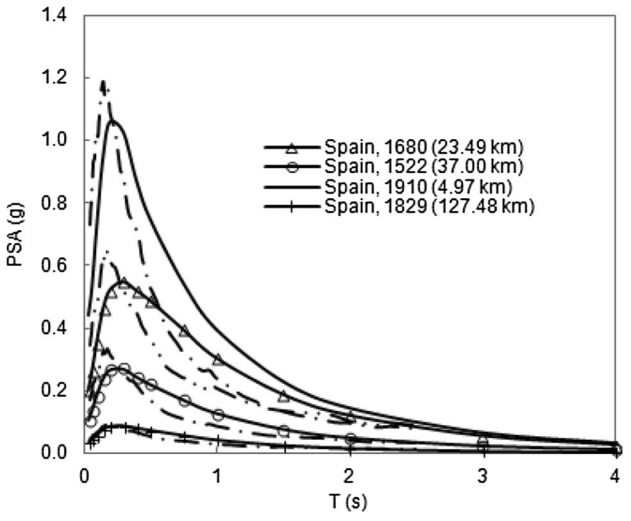

Fig. 6 Deterministic spectra of four records using SP96 and using Am05 (in dashed line). In the brackets, the estimated R_{jb} distance used in the Am05 equation is shown

4 Case study

4.1 The Rules dam on the Guadalfeo River

The structure of interest is a large, concrete, arch-gravity dam in the Granada province of southern Spain. This dam has a 620 m crown length and a 500-m radius. The maximum height of the vertical cantilever is 130.33 m (central black block in Fig. 7b), and the downstream and upstream slope faces are 1:0.60 and 1:0.18, respectively. The dam is made from 32 blocks. The seven dark grey blocks in the centre represent the spillway. The reservoir is shown in Fig. 7a [27]. The capacity and area for the maximum operating level of the reservoir are 117.07 Hm^3 and 308 Ha, respectively, whereas the area of the water basin is 1070 km^2.

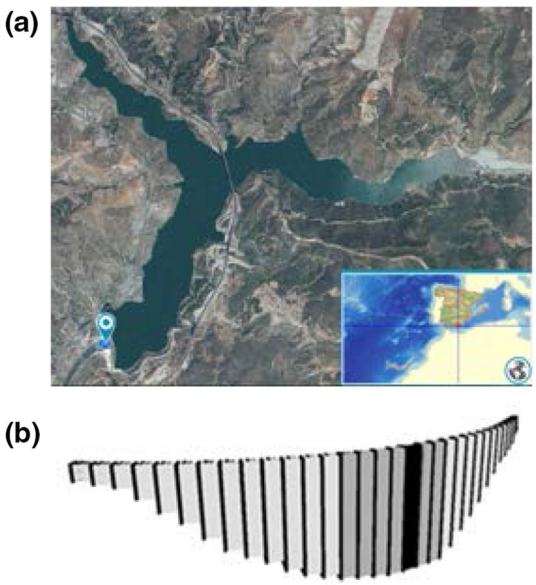

Fig. 7 Position of the Rules dam (36°51′35″ N, 3°29′43″ W) (**a**) and FEA 3D model (**b**)

4.2 Mathematical model

The numerical simulation was made using Finite Element Analysis (FEA) and the gravity method. The two- and three-dimensional FEA (Sap2000 software) [28] methods were used. The discretization of the 2D and 3D models are explained below.

In FEA (3D), the solid elements (32,980 elements) have a dimension of 3.00 m per 2.50 m, and there are 36,925 monolith joints. Those joints are necessary to analyse the nonlinear effects, such as concrete cracking and plastic hinges [29]. In the 3D model, the length of the block is 19.375 m. In FEA (2D), the solid elements (683 elements) have a dimension of 3.01 m per 2.79 m, and there are 765 joints. In the 2D model, the length of the block is 1 m. The solid element has eight nodes; each one has three degrees-of-freedom. In the gravity method (2D), the principal triangle of the central dam block has been considered. The height is 120 m, and the base is 93.6 m. The dam is divided into 48 lift joints with 2.5-m heights. The gravity method has been used only for the 2D analysis; it is based on rigid body equilibrium and on beam theory. The dam, via the 2D analysis, has been idealized as a triangular shape [30, 31] because the transverse behaviour is similar to a thick gravity dam with a large base thickness. The lift joints have homogeneous properties, and the loads are transferred to the foundation only by cantilever; therefore, it does not consider the arch-effect. The foundation

and abutments have rocky stratigraphic profiles; the values of the site geology refer to an average shear wave velocity over 750 m/s. Since the foundation is rocky, the base has been considered fixed, i.e., the direction displacements of all points of the base are constrained. The gravity method does not consider the dam-foundation interaction, and therefore, the constraints are not well-defined (it is enough to insert the foundation parameters, which is explained below). The loads present in the FEA include the dead load, the hydrostatic pressure and the hydrodynamic pressures. In the gravity method, in addition to the three loads, the seismic dead load and uplift load have been applied. In FEA, the hydrodynamic and hydrostatic pressures act normal to the face and are uniform for each solid.

The pseudo-hydrodynamic pressure occurs because the water is linearly compressible and irrotational. Furthermore, the internal viscosity of water is neglected, and the effects of waves at the free surface are omitted [32]. The hydrodynamic pressure of incompressible water (pressure independent of frequency) and the absorption effects of the reservoir bottom [33] have also been studied. In this example, the input data used are E_c = 44.40 GPa (modulus of elasticity of the concrete), γ_c = 24 kN/m^3 (mass density of the concrete), ν_c = 0.20 (Poisson's ratio of the concrete) and ξ_d = 5% (dam damping). In the FEA models, to consider the voids (e.g., galleries, drains and spillways) in the dam body, γ_c is set to 20.64 kN/m^3, i.e., less than 14% of 24 kN/m^3. This difference has been obtained from the ratio of the real weight to the model weight: $(3.6\times10^3\ t)/(4.2\times10^3\ t)=0.86$. To consider the interaction between the substructures, e.g., dam–reservoir–foundation–sediments [34] and dam–abutments, the following data have been used: E_f = 41.55 GPa (modulus of elasticity of the foundation rock), γ_f = 27.47 kN/m^3 (mass density of the foundation rock), ν_f = 0.33 (Poisson's ratio of foundation rock), γ_w = 9.81 kN/m^3 (mass density of water), C_w = 1438 m/s (velocity of pressure waves) and α_w = 0.41 (wave reflection coefficient for reservoir bottom materials).

5 Results of the dynamic analysis

The recorded data must be carefully analyzed by performing the appropriate corrections and focusing on seismic demands [35, 36]. The controlling earthquakes have been used for this THA. By defining the significant durations [37] for each record, it is possible to select the most influential interval. Figure 8 shows the THA of the vertical stresses (σ_y) at the wall's heel of the dam's central block using three records; it shows the cases of empty and full reservoirs and both dynamic actions (seismic deadweight and hydrodynamics). In this case, the seismic deadweight includes the self-weight. In the analysis, there are slight differences between the analytical (normal stress) and the computational analysis (principal stress). The analytic pressure values are in accordance with those reported in the literature [38]. The principal stresses, due to the wall inclination, are obtained by software [39]. The full reservoir analysis demonstrates that the stresses are lower due to the hydrostatic and uplift negative stresses. However, during the seism, uplift pressures within the crack can be assumed to be zero, and therefore, the σ_y total increases. The constitutive law for compression and tension used for concrete is in accordance with the European Committee for Standardization [40]. The maximum tensile value adopted, which generates significant nonlinear plastic deformations, is f_{ctd} = 1547 kN/m^2 (horizontal dashed line in Figs. 8, 9). Other tensile strengths, which can be used for gravity dams with lower characteristics (f_{ctd} = 960 kN/m^2), are shown in Figs. 8 and 9. For the unfavourable (unf.) full reservoir, when all forces have the same direction, the stresses exceed the ± 960 kN/m^2 value by 174 times in the heel and 558 in the toe. The stress analysis determines potential crack (the crack opens and closes during the earthquake) and plastic hinge formations. For each vibration, the stress analysis accumulates inelastic deformations [41], producing a hysteretic behaviour that depends on dissipated energy. Figure 9 shows the THA

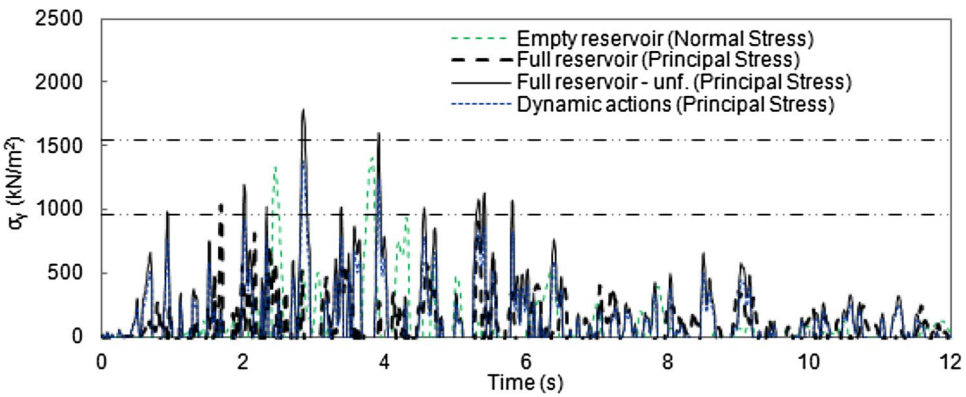

Fig. 8 Dynamic stress at the heel of the wall (singular point in the upstream)

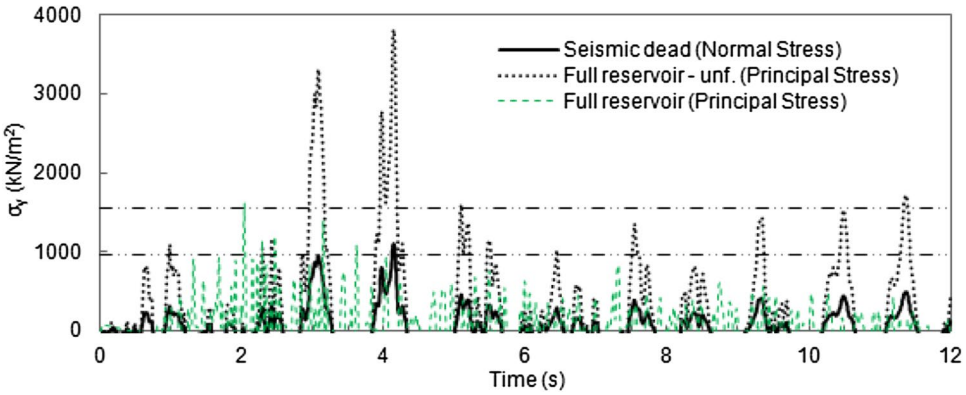

Fig. 9 Dynamic stress at the toe of the wall (singular point in the downstream)

of the stresses in the wall's toe of the dam's central block using two records. The seismic dead weight also includes the self-weight.

The structural analysis provided the following results: T_d is 0.284 s, the second dam period is 0.245 s, and the third dam period is 0.208 s. The first dam-reservoir period is 0.344 s, and the system's (dam-foundation-reservoir) fundamental period, T_s, is 0.393 s (the system damping, ξ_s, is 8.5%). The operating level considered is 113.00 m. The seismic dead weight and the hydrodynamic normal stresses, in relation to the maximum values calculated in this analysis, are less than 31.6% (at one-third of *y*) and 68.4% (at two-thirds of *y*) and 42.1% (at one-third of *y*) and 89.5% (at two-thirds of *y*), respectively. The *y* axis is zero in the bottom of the reservoir. The self-weight and hydrostatic horizontal stresses are − 71.78 kN/m^2 (at the toe), − 239.26 kN/m^2 (at the heel), − 1028.24 kN/m^2 (at the toe), and − 585.09 kN/m^2 (at the heel), respectively. Along the base of the dam, the seismic dead stresses increase, whereas the hydrostatic stresses decrease. The hydrodynamic and hydrostatic pressure effects and the sediment effects have been studied by other authors [42] and, therefore, are not shown here.

6 Conclusions

In this paper, the seismic risk of the Rules dam is evaluated. The possible maximum accelerations that can act against the dam's body are evaluated, and the dam's behaviour has been made explicit. The main conclusions are summarized as follows:

- The analysis has been performed in the site in which the dam is placed. The analysis carried out in this study shows that there are some differences in relation with the Zesis data. However, a precise study "ad hoc" is needed. Different values were only obtained in four zones ($\Delta\lambda_c$, Δb and $\Delta m_{,max}$ range between − 0.31 and 0.23, − 0.75 to 0.67, − 0.2–1.7, respectively). The seismic hazard is high and has a maximum moment magnitude of 6.8. The main differences are due to the recovered data and process uncertainties, e.g., the choice of the operations: homogenization, declustering and completeness.
- The PSHA and the DSHA have been used to define the design parameters. In the Spanish code, the PGA for the area is 0.17 g. In the PSHA, the PGA range is 6–135% higher than 0.17 g. In the DSHA, the range goes up to 200%. By considering the return period of the seismic action, for the no-collapse requirement of 1000 years, 0.25 g of ground acceleration has been calculated for the analysis. This study does not consider the site effects, e.g., amplification, topographic effects, and effect of foundation inhomogeneity [43]. This paper encourages the development of these issues in future research.
- The obtained system values are as follows: a fundamental period of 0.39 s and 8.5% damping. The system represents the interaction between the dam, foundation and water. In the heel, the increase due to dynamic action is 41.67% of the self-weight normal stress and 41.19% of the water principal stress. In the toe, the horizontal stress due to the hydrostatic action in the dam is 36% of the vertical stress. In the dynamic analysis, the maximum vertical principal stress is 3.8 MPa, while in the pseudo-static analysis—a rigid system with a period of vibration equal to zero—it is 2.6 MPa. An important number of inelastic deformations have been observed. The seismic input is obtained from a seismic hazard reanalysis. Since the structure was built (in 2003) before the modern seismogenic zone was created, these calculations and considerations may not be accurate since they were made in the original dam project.

Acknowledgements The authors thank the native English speaking editors at American Journal Experts (AJE) for the manuscript review. The third author acknowledges support by CNPq, a Brazilian research funding agency.

Compliance with ethical standards

Funding This study was funded by doctoral school Studii Salamantini of University of Salamanca [reference number 100015235810]. The manuscript revision was funded by the doctoral programme "Geotechnologies applied to construction, energy and industry" of University of Salamanca [reference number J6ZWMC1S].

References

1. Cornell CA (1968) Engineering seismic risk analysis. Bull Seismol Soc Am 58(5):1583–1606
2. Woo G (1996) Kernel estimation methods for seismic hazard area source modeling. Bull Seismol Soc Am 86(2):353–362
3. Gaspar-Escribano JM, Rivas-Medina A, Parra H, Cabañas L, Benito B, Ruiz Barajas S, Martínez Solares JM (2015) Uncertainty assessment for the seismic hazard map of Spain. Eng Geol 199:62–73
4. Faccioli E, Paolucci R (2005) Elementi di sismologia applicata all'ingeneria. Pitagora Editrice, Bologna
5. Comisión Permanente de Normas Sismorresistentes (2002) Norma de construcción sismorresistente: Parte general y edificación. Ministro de Fomento, Madrid
6. Gutenberg B, Richter CF (1944) Frequency of earthquakes in California. Bull Seismol Soc Am 34(4):185–188
7. Zhan Z (2017) Gutenberg-Richter law for deep earthquakes revisited: a dual-mechanism hypothesis. Earth Planet Sci Lett 461:1–7
8. IGME (2015) ZESIS: Base de Datos de Zonas Sismogénicas de la Península Ibérica y territorios de influencia para el cálculo de la peligrosidad sísmica en España. http://info.igme.es/zesis. Accessed June 2016
9. López Casado C, Sanz de Galdeano C, Delgado J, Peinado MA (1995) The b parameter in the Betic Cordillera, Rif and nearby sectors. Relations with the tectonics of the region. Tectonophysics 248:277–292
10. Instituto Geográfico Nacional (IGN) (2017). http://www.ign.es/web/ign/portal/sis-catalogo-terremotos. Accessed 14 June 2016
11. Instituto Andaluz de Geofísica (IAG) (2017). http://iagpds.ugr.es/
12. Sabetta F, Pugliese A (1996) Estimation of response spectra and simulation of nonstationary earthquake ground motions. Bull Seismol Soc Am 86(2):337–352
13. Ambraseys NN, Simpson KA, Bommer JJ (1996) Prediction of horizontal response spectra in Europe. Earthq Eng Struct Dyn 25:371–400. doi:10.1002/(SICI)1096-9845(199604)25:4<371::AID-EQE550>3.0.CO;2-A
14. Ambraseys NN, Douglas J, Sarma SK, Smit PM (2005) Equations for the estimation of strong ground motions from shallow crustal earthquakes using data from Europe and the Middle East: Horizontal peak ground acceleration and spectral acceleration. Bull Earthq Eng 3(1):1–53. https://doi.org/10.1007/s10518-005-0183-0
15. Berge-Thierry C, Cotton F, Scotti O (2003) New empirical response spectral attenuation laws for moderate European earthquakes. J Earthquake Eng 7(2):193–222. https://doi.org/10.1080/13632460309350446
16. Benito B, Gaspar-Escribano JM (2007) Ground motion characterization and seismic hazard assessment in Spain: context, problems and recent developments. J Seismolog 11:433–452. https://doi.org/10.1007/s10950-007-9063-1
17. Scordilis EM (2006) Empirical global relations converting M_s and m_b to moment magnitude. J Seismolog 10:225–236. https://doi.org/10.1007/s10950-006-9012-4
18. Benito MB, Navarro M, Vidal F, Gaspar-Escribano J, García-Rodríguez MJ, Martínez-Solares JM (2010) A new seismic hazard assessment in the region of Andalusia (Southern Spain). Bull Earthq Eng 8:739–766. https://doi.org/10.1007/s10518-010-9175-9
19. Cabañas L, Rivas-Medina A, Martínez-Solares JM, Gaspar-Escribano JM, Benito B, Antón R, Ruiz-Barajas S (2015) Relationships between M_w and other earthquake size parameters in the Spanish IGN seismic catalog. Pure Appl Geophys 172:2397–2410. https://doi.org/10.1007/s00024-014-1025-2
20. Gardner JK, Knopoff L (1974) Is the sequence of earthquakes in southern California, with aftershocks removed, Poissonian? Bull Seismol Soc Am 64(5):1363–1367
21. Ordaz M, Aguilar A, Arboleda J (2007) Crisis2007 (Version 5.4). Unam, Coyoacán
22. Sanz de Galdeano C, Peláez Montilla JA, López Casado C (2003) Seismic potential of the main active faults in the Granada basin (southern Spain). Pure Appl Geophys 160:1537–1556. https://doi.org/10.1007/s00024-003-2359-3
23. Luzi L, Puglia R, Russo E, ORFEUS WG5 (2016) Engineering Strong Motion Database, version 1.0. Istituto Nazionale di Geofis e Vulcanol Obs Res Facil Eur Seismol. doi:10.13127/ESM. http://esm.mi.ingv.it. Accessed 16 December 2016
24. Seismosignal (Version 4.0.0) (2010). Seismosoft Ltd, Pavia
25. García-Mayordomo J, Insua-Arévalo JM (2011) Seismic hazard assessment for the Itoiz dam site (Western Pyrenees, Sapin). Soil Dyn Earthq Eng 31:1051–1063. https://doi.org/10.1016/j.soildyn.2011.03.011
26. Gaspar-Escribano JM, Navarro M, Benito B, García-Jerez A, Vidal F (2010) From regional- to local-scale seismic hazard assessment: examples from Southern Spain. Bull Earthq Eng 8:1547–1567. https://doi.org/10.1007/s10518-010-9191-9
27. SNCZI-Inventario de Presas y Embalses (2017). http://sig.mapama.es/snczi/visor.html
28. Sap2000 (Version 16.0.0 Plus) (2013) Computers and Structures, Inc, California/New York
29. Durieux JH, Van Rensburg BWJ (2016) Development of a practical methodology for the analysis of gravity dams using the non-linear finite element method. J S Afr Inst Civil Eng 58(2):2–13
30. Khosravi S, Heydari MM (2013) Modelling of concrete gravity dam including dam-water-foundation rock interaction. World Appl Sci J 22(4):538–546. https://doi.org/10.5829/idosi.wasj.2013.22.04.551
31. Kaveh A, Ghaffarian R (2015) Shape optimization of arch dams with frequency constraints by enhanced charged system search algorithm and neural network. Int J Civil Eng 13(1):102–111. https://doi.org/10.22068/IJCE.13.1.102
32. Chakrabarti P, Chopra AK (1973) Earthquake analysis of gravity dams including hydrodynamic interaction. Earthq Eng Struct Dyn 2:143–160. https://doi.org/10.1002/eqe.4290020205
33. García F, Aznárez JJ, Padrón LA, Maeso O (2016) Relevance of the incidence angle of the seismic waves on the dynamic response of arch dams. Soil Dyn Earthq Eng 90:442–453
34. Tarinejad R, Pirboudaghi S (2015) Legendre spectral element method for seismic analysis of dam-reservoir- interaction. Int J Civil Eng 13(2):148–159. https://doi.org/10.22068/IJCE.13.2.148
35. Wang G, Wang Y, Lu W, Yan P, Zhou W, Chen M (2016) A general definition of integrated strong motion duration and its effect on seismic demands of concrete gravity dams. Eng Struct 125:481–493
36. Hariri-Ardebili MA, Mirzabozorg H, Kianoush R (2014) Comparative study of endurance time and time history methods in seismic analysis of high arch dams. Int J Civil Eng 12(2):219–236
37. Peláez JA, Delgado J, López Casado C (2005) A preliminary probabilistic seismic hazard assessment in terms of Arias intensity in southeastern Spain. Eng Geol 77:139–151. https://doi.org/10.1016/j.enggeo.2004.09.002

38. Millán MA, Young YL, Prévost JH (2002) The effects of reservoir geometry on the seismic response of gravity dams. Part 1: Analytical model. Earthq Eng Struct Dyn 00:1–6
39. Leclerc M, Léger P, Tinawi R (2004) Cadam (Version 1.4.14). CRSNG/Hydro-Québec/Alcan, Montréal
40. European Committee for Standardization (2004) Design of concrete structures. Part 1–1: general rules and rules for buildings. CEN, Brussels
41. Alembagheri M (2016) Earthquake damage estimation of concrete gravity dams using linear analysis and empirical failure criteria. Soil Dyn Earthq Eng 90:327–339
42. Zacchei E, Molina JL, LRF Brasil MR (2017) Seismic hazard and structural analysis of the concrete arch dam (Rules dam on Guadalfeo River). Procedia Eng 199:1332–1337. http://dx.doi.org/10.1016/j.proeng.2017.09.334
43. Joshi SG, Gupta ID, Murnal PB (2015) Analyzing the effect of foundation inhomogeneity on the seismic response of gravity dams. Int J Civil Struct Eng 6(1):11–24. https://doi.org/10.6088/ijcser.6002